Fuel 235 (2019) 627–638

Contents lists available at ScienceDirect

Fuel

journal homepage: www.elsevier.com/locate/fuel

Full Length Article

Comparison of ESEM and physical properties of virgin and laboratory aged asphalt binders

Peter Mikhailenko[a,*], Changjiang Kou[a,b], Hassan Baaj[a], Lily Poulikakos[c], Augusto Cannone-Falchetto[d], Jeroen Besamusca[e], Bernhard Hofko[f]

[a] Centre for Pavement and Transportation Technology (CPATT), University of Waterloo, Canada
[b] College of Civil Science and Engineering, Yangzhou University, China
[c] Empa, Swiss Federal Laboratories for Materials Testing and Research, Laboratory for Road Engineering/Sealing Components, Dubendorf, Switzerland
[d] Technische Universität Braunschweig, ISBS, Braunschweig, Germany
[e] Kuwait Petroleum Research and Technology, Europoort Rotterdam, The Netherlands
[f] Technical University of Vienna, Vienna, Austria

ARTICLE INFO

Keywords:
Asphalt binder
Aging
Environment Scanning Electron Microscopy (ESEM)
Microstructure
DSR
Penetration
Softening point

ABSTRACT

The physical and microstructural properties of four straight run asphalt binders were examined and compared in combination with short term aging (RTFOT) and long-term (PAV) laboratory aging. RTFOT aging was conducted at temperatures of 123, 143 and 163 °C. The physical testing parameters included penetration, softening point and Dynamic Shear Rheology (DSR) complex shear modulus and phase angle at 10 °C. The binders selected came from four different sources and had the same penetration grading (70/100). They all showed an increase in stiffness with aging, including with the increase in RTFOT temperatures and especially with PAV aging. The microstructural evolution of the binder was examined by Environmental Scanning Electron Microscopy (ESEM) on aged binders at 123 and 163 °C. The physical changes with aging corresponded to an evolution in the binders' 'fibril' microstructure under ESEM, as a result of electron beam exposure, with the microstructure getting denser with PAV aging. This densification (fibril area) of the microstructure was quantified with image analysis for the virgin and RTFOT aged samples, and the fibril formation time was also measured. The asphalt binders showed varied ESEM 'fingerprints' and aged in different ways. The ESEM 'formation time' and 'fibril area' of the binders generally showed good correlation with the physical properties, although this was not the case for all of the binders due to their unique aging characteristics.

1. Introduction

Despite the widespread use of asphalt binders, there remains a lot to be understood about its nature [1]. Although asphalt binder (bitumen) only represents around 5% of the mass of typical hot mix asphalt mixtures, it plays a key role in determining the behaviour and the performance of the mixture and has a significant impact on the performance of the pavement structure [2]. Furthermore, it is the binder that undergoes physical and chemical aging during the pavement service life [3], making its further understanding of vital importance.

A promising but not yet well understood technique for observing the nature of asphalt binder is Environmental Scanning Electron Microscopy (ESEM) [4]. ESEM is designed to study wet, and oily materials as it allows observations of such materials in their natural state without de-oiling procedures required for the vacuum environment of a conventional Scanning Electron Microscope (SEM). The image obtained by the ESEM is a result of the interaction of the electron beam with the sample at an atomic level. The secondary electrons that are used in this study are emitted by the sample due to the interaction with the primary electron beam and they represent the sample topography. The volume of interaction between the electron beam and the sample is more at the surface resulting in more electrons escaping from the peaks than from the valleys resulting in peaks being brighter and valleys dark [5]. When an asphalt binder sample is placed in the ESEM, the subjection of the sample to an electron beam (in secondary electron mode), causes it to form 'fibril' microstructures that eventually stabilize. The parameters retrieved from this could be i) the density of the fibril + microstructure [6], ii) the size and shape of the fibrils [7] and iii) the amount of time

* Corresponding author at: Centre for Pavement and Transportation Technology (CPATT), Department of Civil & Environmental Engineering, University of Waterloo, 200 University Ave W, Waterloo, ON N2L 3G1, Canada.
E-mail address: p2mikhai@uwaterloo.ca (P. Mikhailenko).

https://doi.org/10.1016/j.fuel.2018.08.052
Received 31 May 2018; Received in revised form 8 August 2018; Accepted 11 August 2018

the structure takes to form them and stabilize [8].

There have been a few studies on asphalt binder with this technique that have confirmed the formation of the fibril microstructure [7]. Initially, researchers assumed that the structures developed as a result of electron exposure was related to the heaviest molecules in the binder (i.e. asphaltenes). It has since been proposed that they correspond to a part of the maltenes (intermediate to light molecular weight) fraction and possibly a part of the asphaltenes [9]. The microstructure has been found to evolve with both binder aging and tensile forces [4]. Furthermore, mixes of virgin and aged binders have been shown to produce hybrid fibril microstructures in ESEM, sharing the properties of both parent binders [10]. The microstructure has also been found to form at observation temperatures as low as −80 °C [11].

There are still questions regarding the reasons why the fibril microstructure forms and what it represents. A similar phenomenon has been observed where a non-conductive organic material is bombarded with electrons [12]. In its conventional use, an SEM would be used on a conductive material or one with a conductive coating, where the electrons (energy) sent to the material would mostly pass through the sample [13]. Asphalt binders are too viscous to be treated with the coating successfully [14]. When the binder is exposed to the electron beam, inelastic collisions between the materials occur and the energy stays inside the sample [15]. From the understanding of this phenomenon in other organic, viscous and volatile materials observed with the electron beam, it is known that one of the effects of this is a significant amount of local heating being generated [16]. Another is the addition to the dispersion of certain molecules like aliphatics, which would be less rigid than the aromatic parts of the binder [17]. A study looking at asphalt binder in this context found a slightly higher aliphatic signal in the area where the irradiation occurred, but a stronger aromatics presence on the fibrils themselves [11].

Despite some very interesting results, the relation of the ESEM findings to asphalt binder physical performance and aging needs to be further understood. This study is part of a larger inter-laboratory study of the RILEM Technical Committee 252 CMB. The virgin and aged binders were subject to both physical testing (Penetration, Softening Point (R&B), Rheology (DSR)) and chemical testing using FTIR performed by ten laboratories in five countries [18]. The objective of the current paper is to analyse these same four straight run asphalt binders that have the same penetration grade, and the evolution of their microstructures after short term aging (RTFOT) and subsequent long-term (PAV) laboratory aging. The ESEM analysis was performed by the University of Waterloo and the binder samples were aged by Empa. This study will allow the authors to: i) validate previous findings on the evolution of aged binder under ESEM, ii) understand the differences of straight run binders from different sources under ESEM and iii) attempt to find a correlation between the physical properties of the binder (penetration, softening point, rheology) and the findings of the ESEM analysis. Overall, this would allow for the validation of the ESEM findings and a better understanding of how they can be interpreted, ultimately giving us further insight into the nature of asphalt binder.

2. Materials and methods

2.1. Materials

2.1.1. Asphalt binders

Four 70/100 penetration specified asphalt binders (EN 12591) from different crude sources were used in this study and identified as B501, B502, B503 and B504. Table 1 provides the properties of the four binder samples according to European Standards (EN 1426, 1427) and the US Performance Grade Specifications (AASHTO M 320-10). The penetration and softening point of the binders was very similar, with B502 being somewhat stiffer (67 1/10 mm) and B504 being somewhat less stiff (81 1/10 mm). The performance grading of the binders was 64–22, except for B501, which graded slightly higher at 70–22.

Table 1
Properties of asphalt binder samples.

Sample	Penetration at 25 °C [1/10 mm]	Softening Point [°C]	PG
B501	77	46.4	70–22
B502	67	47.6	64–22
B503	79	46.3	64–22
B504	81	45.5	64–22

2.2. Methods

2.2.1. Laboratory binder aging

The entire set of binders was short- and long-term aged. Short-term aging was performed according to the RTFOT method (EN 12607-1) with a duration of 75 min. In addition to the standard RTFOT temperature of 163 °C, two additional temperatures, 143 °C and 123 °C, were used to isolate and evaluate the effect of temperature on the aging process. The choice of reduced temperatures was based on warm mix asphalt technologies, which were looked at in a parallel study. Long-term aging was conducted using the PAV device (EN 14769). It was carried out after RTFOT at a temperature of 100 °C and an air pressure of 2.1 MPa for 20 h The RTFOT and PAV have been standard laboratory asphalt aging methods for decades [19].

2.2.2. Penetration, ring and ball

To relate to the different aging effects with standard tests, conventional asphalt binder testing, which is well correlated with bitumen aging [18], was performed. The softening point test according to EN 1427 which represents the consistency at high temperatures. The penetration was tested according to EN 1426 and represents the consistency at intermediate temperatures. Values of penetration and softening point were determined for all asphalt binder samples. Although penetration and softening point are empirical methods they still indicate performance of regular unmodified asphalt binder and are used for product classification of asphalt binders according to European Standards.

2.2.3. Dynamic Shear Rheology

The Dynamic Shear Rheometer (DSR) was used to measure the rheological behaviour of the binder samples under oscillatory sinusoidal loading. The linear viscoelastic (LVE) parameters [20,21] such as complex shear modulus $|G^*|$ and phase angle δ, can be obtained over a wide range of temperatures and frequencies, based on a standard testing procedure. In the present study, DSR testing was carried out with a parallel-plate geometry with an 8 mm diameter and 2 mm gap for temperatures between −10 °C and +40 °C and a 25 mm diameter and 1 mm gap from +30 °C to +80 °C. The tests were carried out with temperature gradients of 10 °C and a frequency sweep from 0.1 Hz to 10 Hz at each temperature. Not all the laboratories were able to perform the tests at the lowest temperatures, so the sample sizes varied. The ESEM testing was conducted at the University of Waterloo on the binders aged at Empa.

2.2.4. Environmental Scanning Electron Microscopy

According to a protocol developed previously [8], the binders were softened by placing them inside covered containers and heating them in an oven for approximately 1 h at 110 °C. Approximately 0.1 g was subsequently poured from the containers into 8 mm diameter sample mold using a spatula and the sample was flattened by holding the mold on a hotplate at 150 °C for approximately 10 s for the virgin binder and up to 30 s for the stiffer aged binders. These temperatures and heating times were kept to a minimum so as to not age the asphalt binder, while still having it malleable enough to transfer to the mold. The samples were stored at a low temperature of 7 °C for 24 h in order to keep aging and changes to the microstructure to a minimum, before observations.

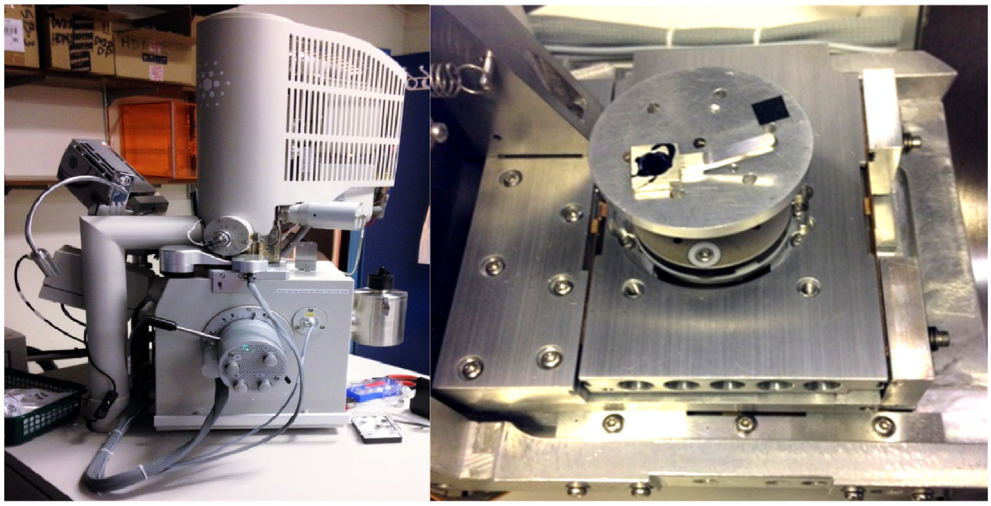

Fig. 1. ESEM Apparatus (left) and one sample on the holder on the ESEM Stage (right).

The observations were conducted at room temperature immediately after being removed from the cooler with a FEI Quanta 250 FEG ESEM (Fig. 1). The observation parameters were an acceleration voltage of 20 keV, a spot size of 3.5, a chamber pressure of 0.8 mbar in low vacuum mode, and a magnification of 1000× in secondary electron (SE) mode.

3. Results

3.1. Physical properties

3.1.1. Penetration, ring and ball

The physical properties results of all asphalt binders with the three different aging regimes are a combined effort of nine labs of the different participants in a RILEM Round Robin. Most participants analysed two different RTFOT aging temperatures. The results for penetration are shown in Fig. 2 and softening point in Fig. 3. The diagrams show the mean value and error bars of the results.

Although the variability for the values of penetration and softening point increases with a higher degree of aging, the trend is clear. The influence of temperature is shown in a decrease of penetration (harder material) and an increase of softening point. The change in penetration and softening point is almost linear with temperature increase in short term conditioning (RTFOT) while the influence of long term conditioning (RTFOT 123 °C/PAV) shows a sharper variation. Combining the RTFOT at 143 °C and PAV results are almost similar with combining RTFOT at 163 °C and PAV. This might indicate a higher degree of chemical reaction, possibly with oxygen, that occurs from 143 °C.

Asphalt binder 502 shows different results in penetration and softening point under laboratory aging compared to the other three asphalt binders with higher softening point and lower penetration, but the effect of aging is similar to other binders

3.1.2. Dynamic Shear Rheology

Based on the time–temperature superposition principle and on the Christensen-Anderson-Marasteanu (CAM) model [22], the experimental

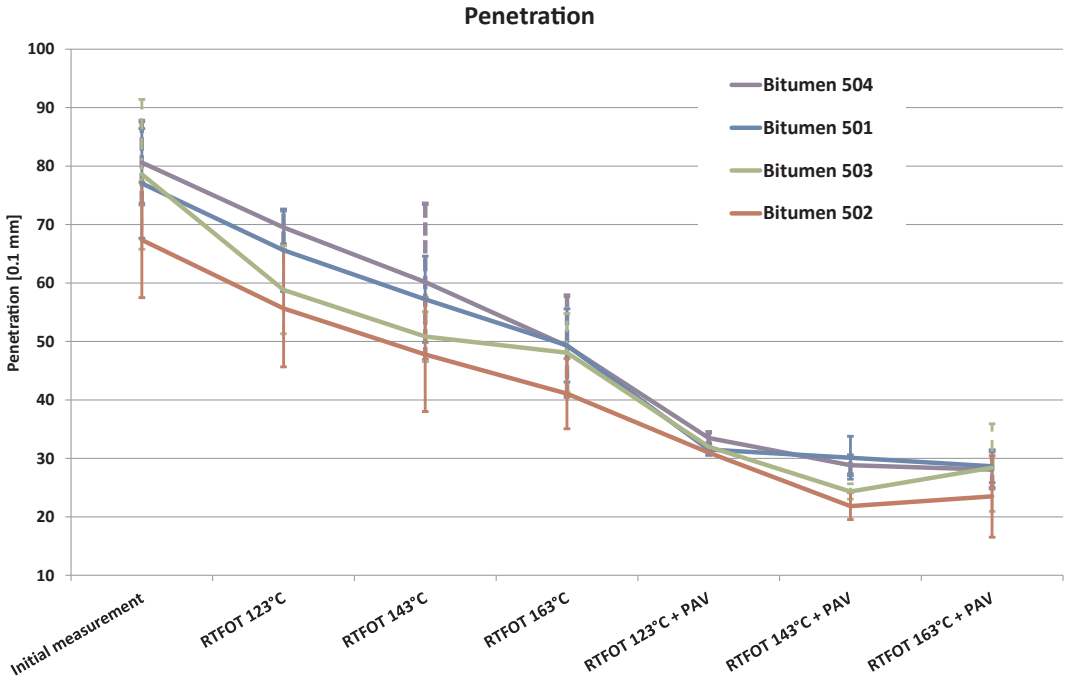

Fig. 2. Penetration values of different asphalt binders at different aging regiments.

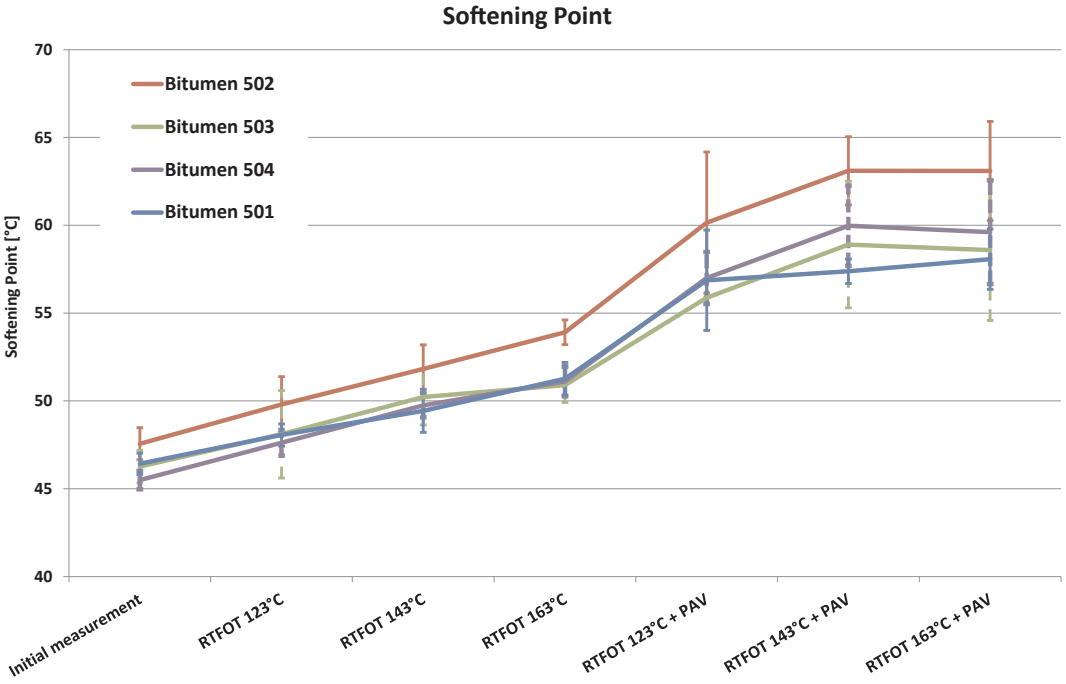

Fig. 3. Softening Point values of different asphalt binders at different aging regiments.

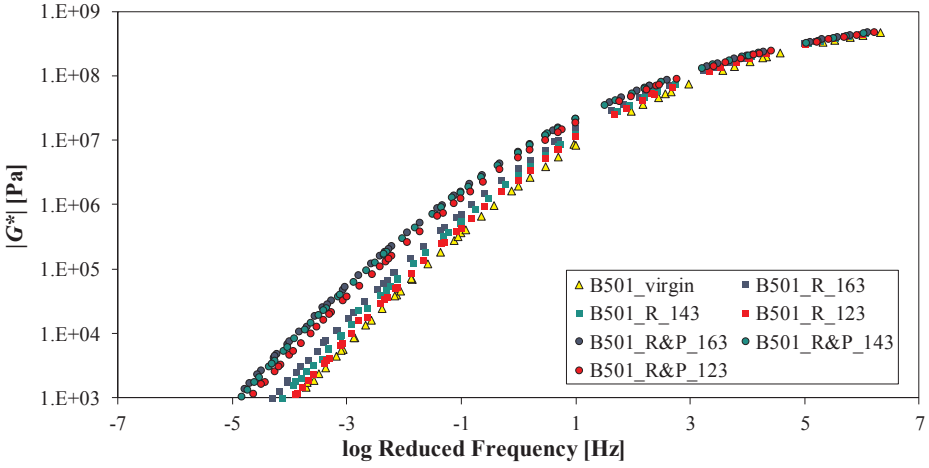

Fig. 4. Master curves of the complex shear modulus for asphalt binder B501 at reference temperature of 10 °C.

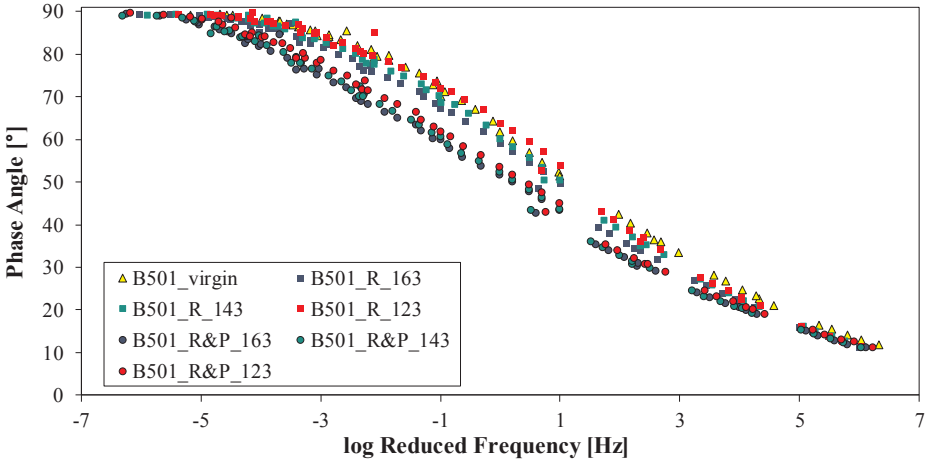

Fig. 5. Master curves of the phase angle for asphalt binder B501 at reference temperature of 10 °C.

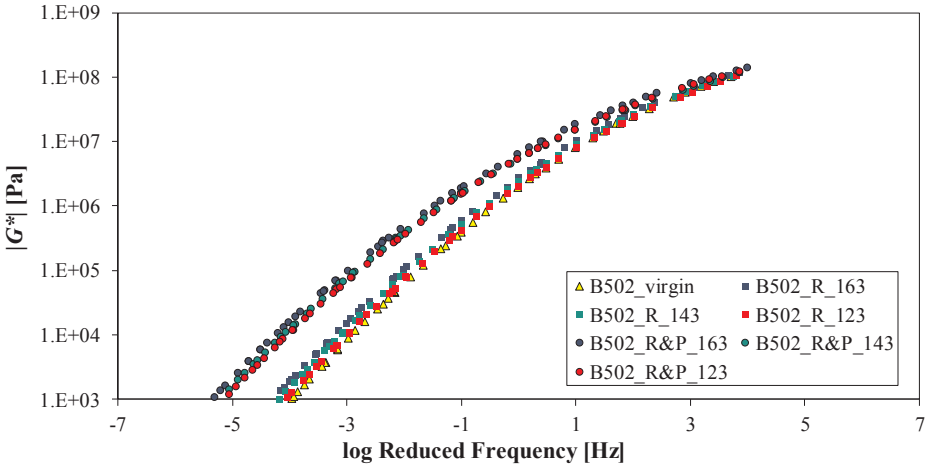

Fig. 6. Master curves of the complex shear modulus for asphalt binder B502 at reference temperature of 10 °C.

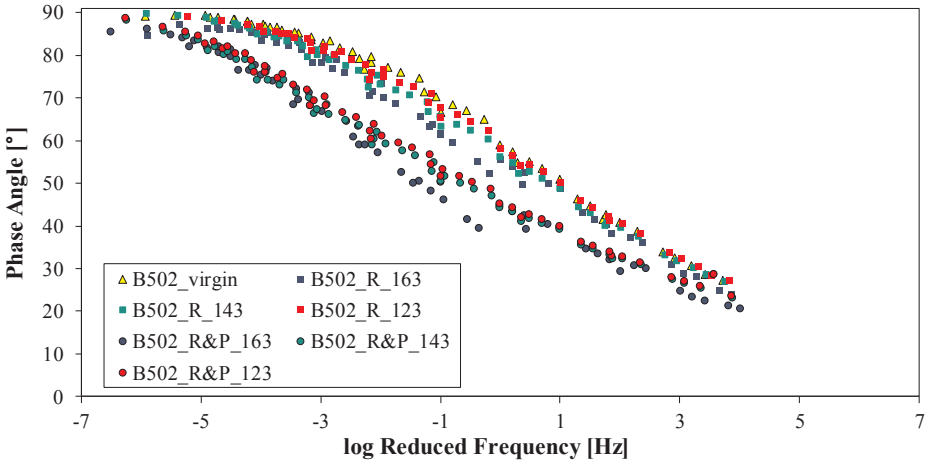

Fig. 7. Master curves of the phase angle for asphalt binder B502 at reference temperature of 10 °C.

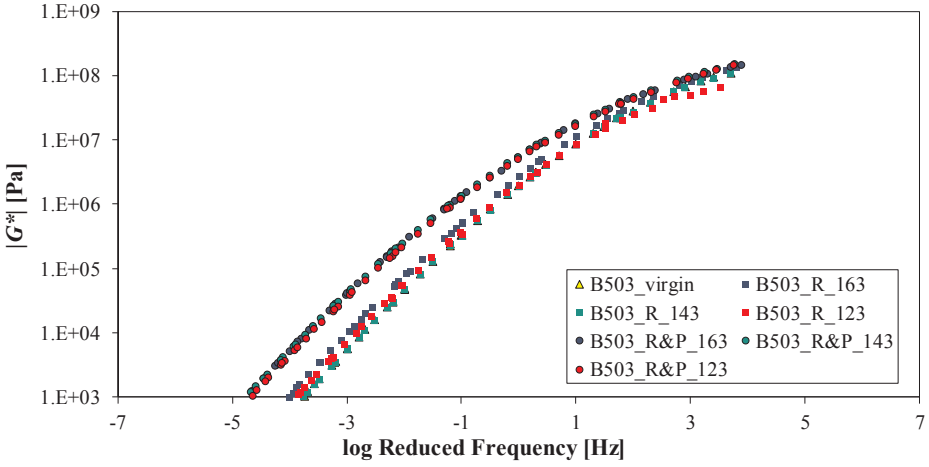

Fig. 8. Master curves of the complex shear modulus for asphalt binder B503 at reference temperature of 10 °C.

DSR (AASHTO T 315-12) measurements were used to generate the master curves of complex modulus, |G*|, and phase angle, δ. Given the specific experimental design selected for the round robin test, each participating laboratory performed the rheological characterization only on a subset of aging conditions, while few participants completed the DSR measurement for all aging temperatures for every binder. For this reason, Figs. 4, 5, 10 and 11 present the master curves calculated with the results obtained from a single laboratory (TU Braunschweig) on asphalt binders 501 and 504, while Figs. 6–9 show the evolution of $|G^*|$ and δ for asphalt binder 502 and 503 derived from the experimental data of two different laboratories.

It must be remarked that only for asphalt binders 501 and 504, low temperature tests down to the lowest temperatures were only performed for binders 501 and 504. This is not the case for the remaining

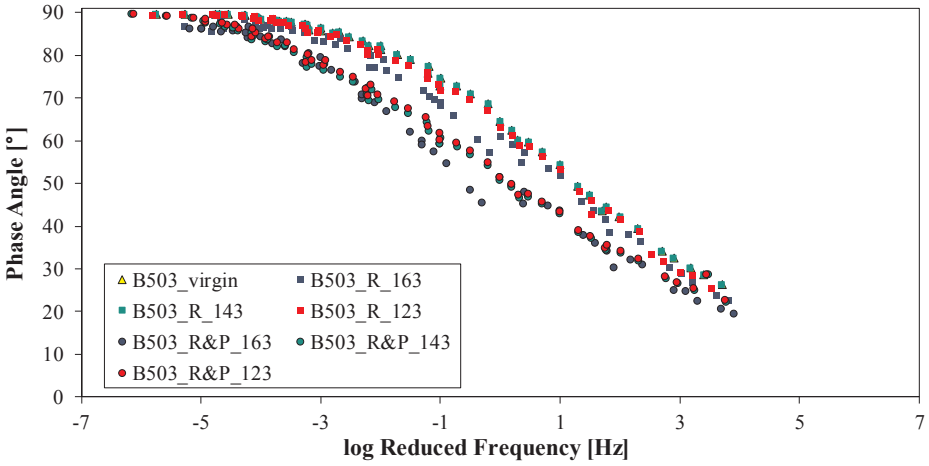

Fig. 9. Master curves of the phase angle for asphalt binder B503 at reference temperature of 10 °C.

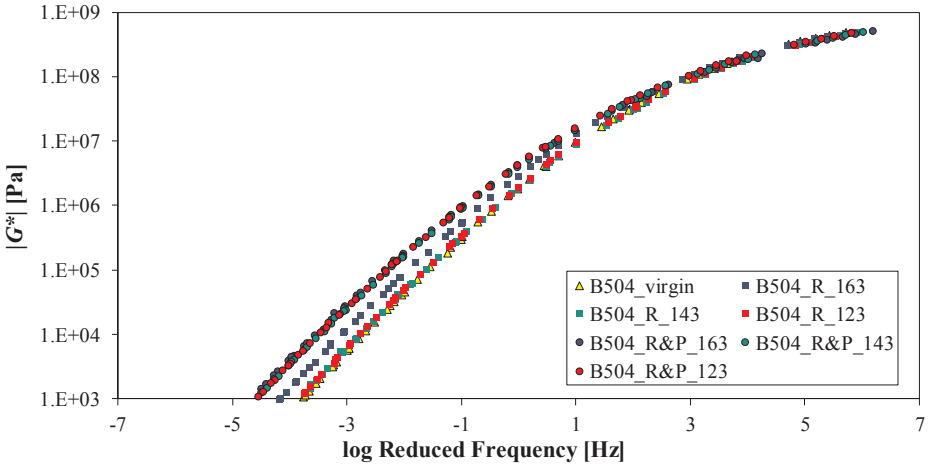

Fig. 10. Master curves of the complex shear modulus for asphalt binder B504 at reference temperature of 10 °C.

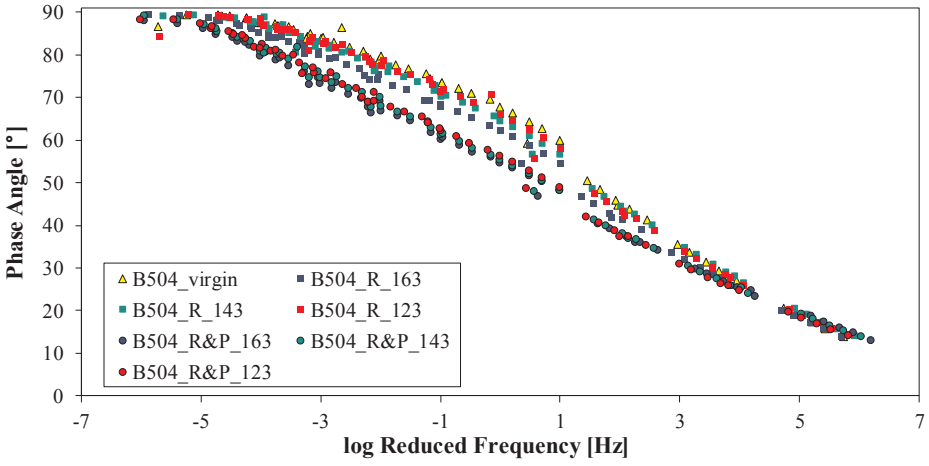

Fig. 11. Master curves of the phase angle for asphalt binder B504 at reference temperature of 10 °C.

binders: 502 and 503. Therefore, the corresponding master curves extend over a narrower frequency range.

A visual inspection of the master curves suggests a substantial difference between the behaviour of the short and long term aged binders. This is clearly noticeable in the low frequency – high temperature domain for the complex modulus, and at intermediate frequency for the phase angle. As expected, at high frequency and low temperature, the complex modulus tends to converge to an asymptotic value close to 1 GPa (binders 501 and 504). It must be mentioned that the use of a 10 °C temperature gradient for DSR testing resulted in master curves with small gaps, which are more remarkable in the case of the phase angle. A simple statistical comparison confirms a substantial different material response between short and long-term aging. Within these two aging conditions (RTFOT and PAV), a significant effect is observed only

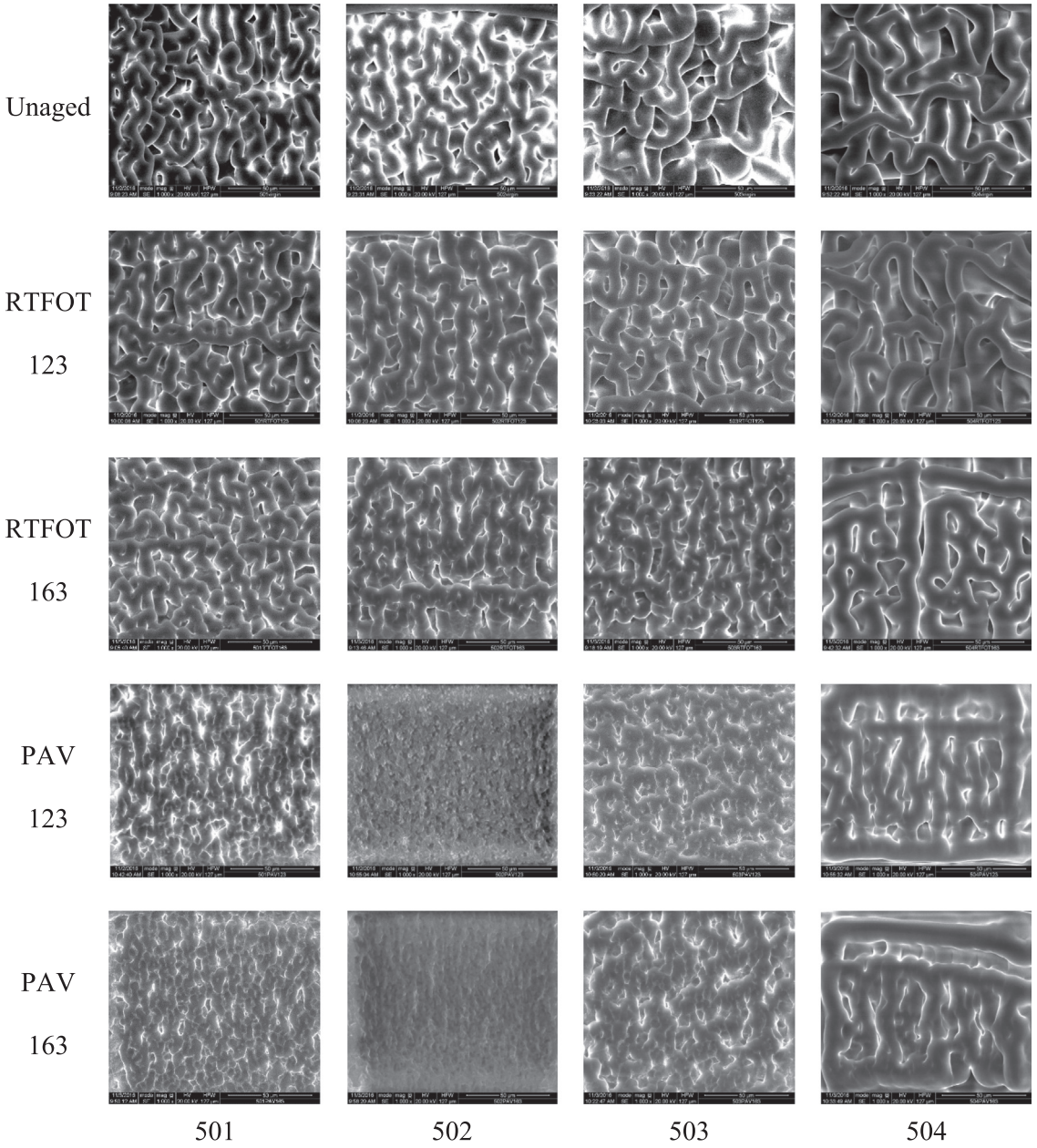

Fig. 12. ESEM images of asphalt binders under different aging conditions.

when a decrease of 40 °C is imposed during the RTFOT aging procedure, confirming the importance of RTFOT aging temperature.

Generally, the rheological behaviour of the binders is similar, with small differences. Notably, the short term RTFOT aging at 163 °C has a more significant aging effect in terms of G* than for RTFOT at 123 °C/143 °C for binder 504, while all binders show this differentiation in the phase angle.

3.2. ESEM microstructure

3.2.1. ESEM microstructure

The irradiation of the binder samples by the ESEM electron beam over a period of time produces a fibril structure. The images of the resulting fibril structure for all of the virgin and aged binders from one lab are shown in Fig. 12. All of the unaged binders have a relatively a looser structure with thicker fibrils and show an evolution of the fibrils with aging. The RTFOT aging at 123 °C does not seem to induce much fibril evolution to the virgin binder, while the structure does appear to become denser (smaller diameter that covers the surface) with RTFOT aging at 163 °C. The structures for all of the binders evolve much more significantly with PAV aging, with the structure getting much denser, especially with binder 502. Binders 501 and 503 show a similar evolution with PAV, with the fibrils also getting smaller in diameter. The PAV evolution of binder 504 was unique in that the fibrils did not decrease in diameter significantly, while the structure became denser.

3.2.2. Fibril formation time

The formation time of the fibril structure with ESEM irradiation has been shown to correlate with binder aging [8] and stiffness [6]. It is calculated from observing Video of the image evolution in the ESEM and taking the time for the fibril structure to stabilize, with the results presented in Fig. 13. The formation time of the fibril structure is the shortest with the virgin binder (10–30 s), and increases a moderate amount with RTFOT aging (30–60 s) and then more significantly with the PAV (80–130 s). It also increases with the increase of RTFOT aging temperature. Binder 502 was an exception to this, as the formation time

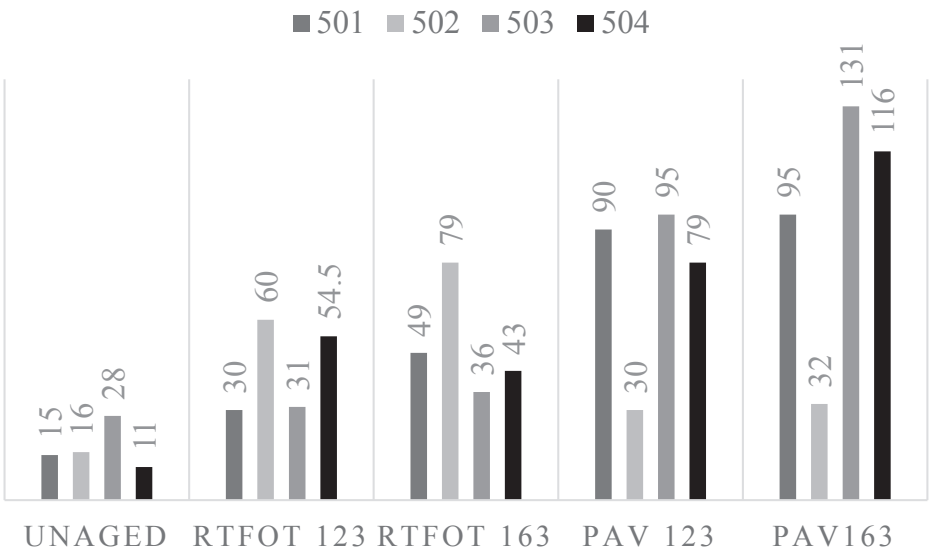

Fig. 13. ESEM fibril microstructure forming (irradiation) time.

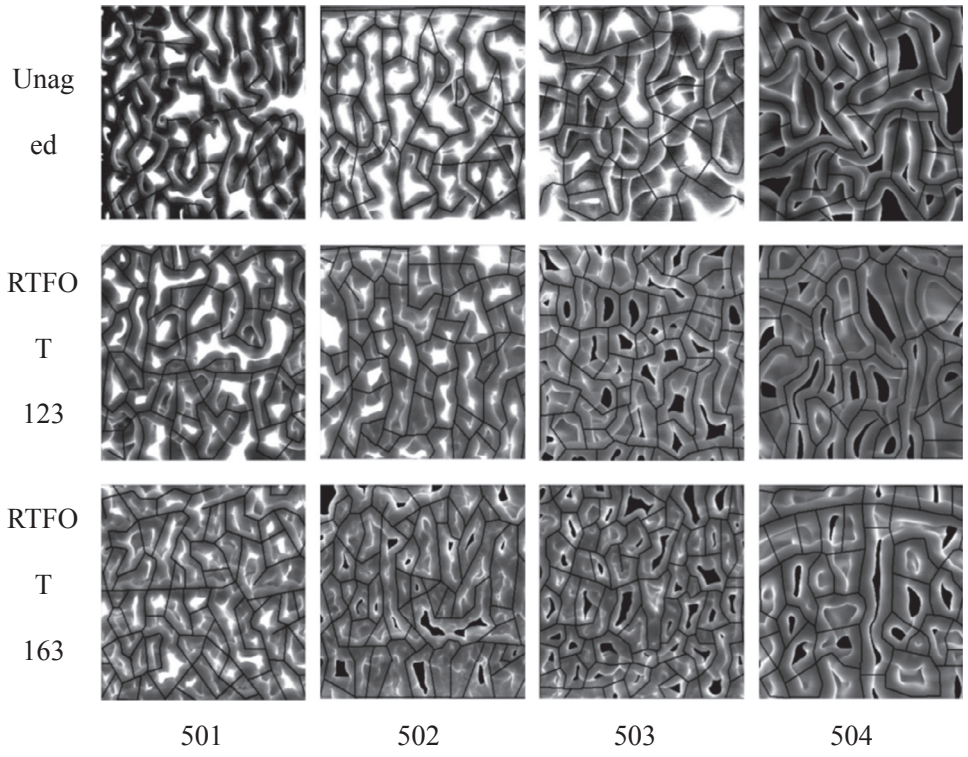

Fig. 14. Examples of sample segmentation for unaged at RTFOT aged binders.

Table 2
Parameters of ESEM Fibril Microstructure.

Binder	Aging Condition	% coverage (density)	Fibril Area (μm)	Fibril Length (μm)	Fibril Diameter (μm)
501	Unaged	88.02	12342.83	1860.41	5.52
	RTFOT 123	89.28	12498.93	1870.05	5.52
	RTFOT 163	96.11	13435.67	2105.59	5.13
502	Unaged	92.63	12989.28	1851.61	5.52
	RTFOT 123	93.59	13145.48	1914.21	5.52
	RTFOT 163	95.60	13488.06	2025.91	5.52
503	Unaged	90.57	12622.67	1473.42	5.52
	RTFOT 123	92.60	12851.32	1842.08	5.46
	RTFOT 163	92.57	13020.68	2241.67	5.52
504	Unaged	89.81	12632.47	1447.79	5.52
	RTFOT 123	93.74	13188.17	1646.31	5.52
	RTFOT 163	92.60	13064.80	1681.45	5.52

increased after the RTFOT aging but was very short after PAV aging, indicating that this parameter cannot be applied in the same way to some binders.

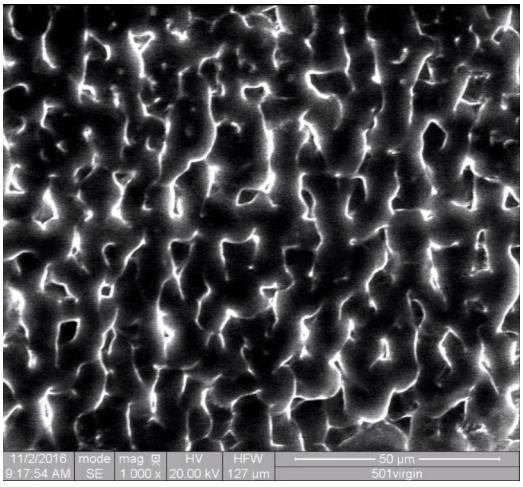

Video.

3.2.3. ESEM image quantification

In order to do quantitative analysis of the images, a process was implemented to extract the microscopic parameters of images, based on similar work with ESEM [7]. The boundary lines around the fibrils were drawn manually using Image Pro Plus in order to create a contrast between fibril and asphalt. The gray-values of asphalt were all substituted with 255 (black). The boundary line images for the virgin and RTFOT aged binders are presented in Fig. 14. Only these binders were analysed as the process was too intensive for the PAV binders, where very many lines would have to be drawn. With this, it was possible to quantify the length (total length of fibrils in image) and area (total fibril area) in a 2-dimensional view (Table 2).

The highest fibril density for the unaged binder for 502 corresponded to the stiffest binder in penetration and softening point. As observed previously, the density of the fibril structure increase with RTFOT aging. The increase was not very significant at 123 °C for binder 501, being much more significant at 163 °C. The increase in density was seen at 123 °C and further at 163 °C for binder 502, while having similar increases after 123 °C and 163 °C for binders 503 and 504. The fibril diameters did not vary significantly between the virgin and RTFOT aged binders.

4. Discussion

Although the binders were all straight run, had similar penetration, softening point and PG grading, the binders had a few differences in terms of the nature and evolution of their microstructures development exposed to ESEM conditions. Binders 501 and 503 appeared and evolved very similarly in terms of their microstructure in the image and formation time, and similarly to straight run binder previously studied with ESEM [8].

Binders 502 and 504 however, appeared distinct from the other two and from each other. The ESEM image for binder 502 after PAV aging appeared very dense and stable, with a very short formation time. Although the formation time has usually been shorter for unaged [10] and more fluid binders [6], in this case, it appears the microstructure was dense enough to not be affected by the irradiation as much and thus, becomes stable very quickly. This higher degree of aging is demonstrated by the PAV aged binder 502 having the lowest penetration and highest softening point values. This also shows that the increase in ESEM microstructural formation time previously found with higher degrees of aging [10], is not applicable for all binders.

For binder 504, the microstructure is also unique from the other three and appears more ‘stringy’. Although the microstructure evolves with RTFOT aging, and PAV aging especially, the microstructure does

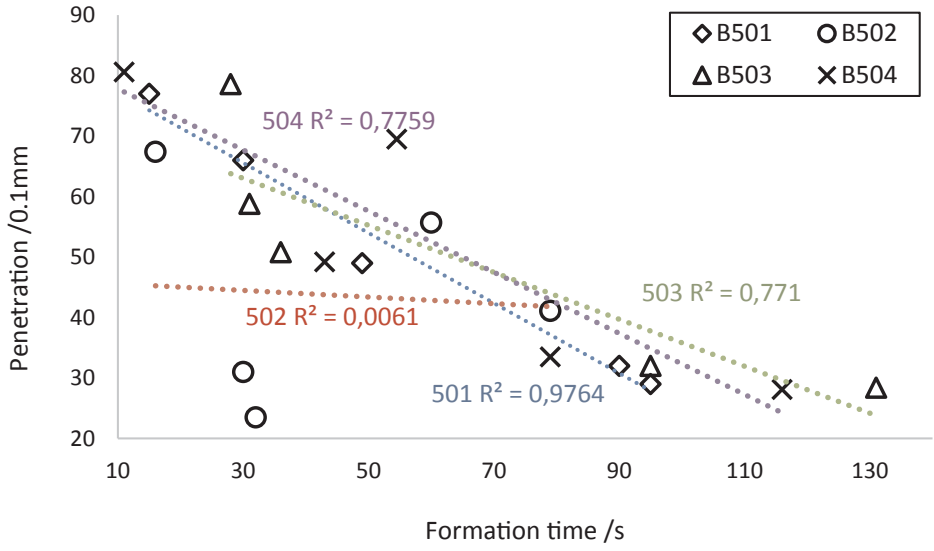

Fig. 15. Correlation of fibril formation time with penetration at 25 °C.

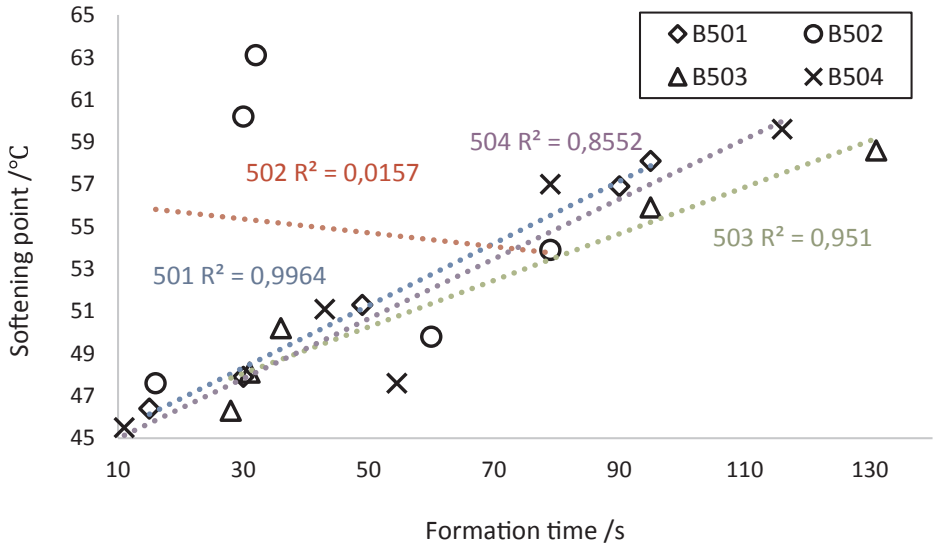

Fig. 16. Correlation of formation time with softening point.

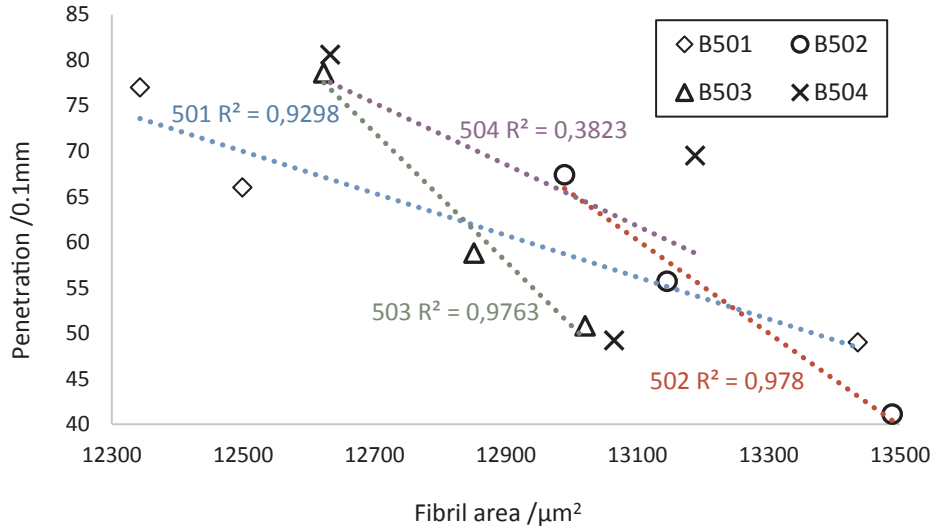

Fig. 17. Correlation of fibril area with penetration at 25 °C.

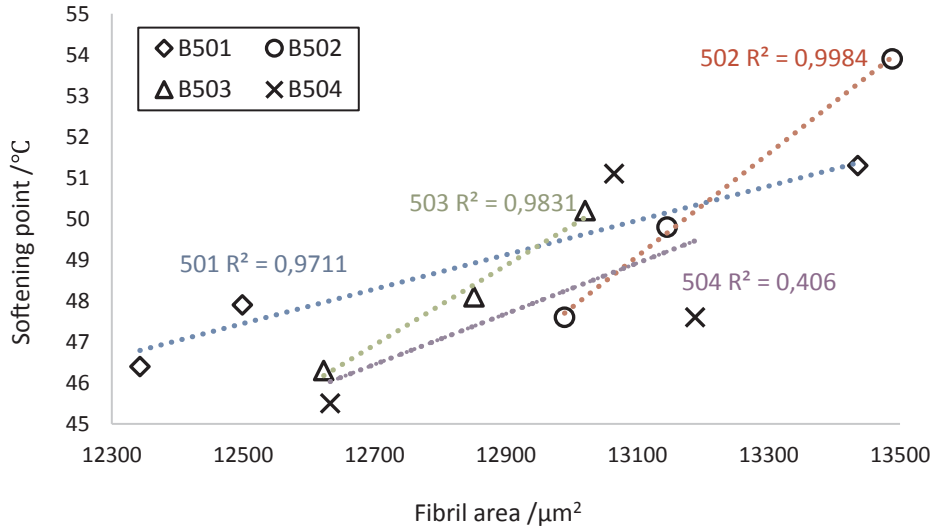

Fig. 18. Correlation of fibril area with softening point.

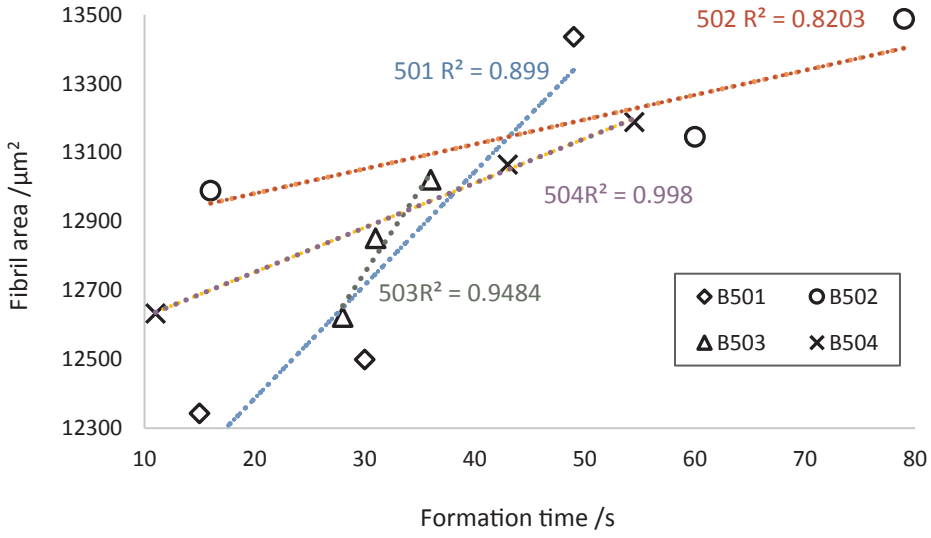

Fig. 19. Correlation of formation time and with fibril area.

not appear to become as dense as those of the other 3 binders. Nevertheless, the binder has similar results to 501 and 503 in terms of physical properties, so more testing is needed to find the reason for the differences. Nevertheless, we can see that similar performing binders can have a very different ESEM 'fingerprint'.

4.1. Parameter correlation analysis

The fibril formation time represents the process of irradiation from the electron beam until the fibril structure tends to stabilize and the fibril area represents the density of the microstructure resulting from this process. Indices like penetration and softening point represent the stiffness of the binder [23]. The correlation of these parameters was analysed for the control samples with the RTFOT and PAV results at 123 and 163 °C in the case of the fibril formation time. For the fibril area, only the control and RTFOT results could be analysed.

The correlation graphs are shown in Figs. 15–19. For formation time, binder 501 correlates well for the limited sample size, with both penetration and softening point with R2 values of around or above 0.9. The correlation is very low for 502 due to the reduction in formation time with PAV aged binders discussed previously. For fibril area, where only the control and RTFOT binders were looked at, the correlation is good for binders 501, 502 and 503 (with penetration), while being non-existent for binder 504. Overall, the correlation between the ESEM and physical parameters was very good for some binders (501) while being more nuanced for others. Finally, the correlation of the ESEM parameters of fibril area and formation time is good as all the R^2 values are above 0.8.

5. Conclusions

The principal conclusions for the 'comparison of ESEM and physical properties in virgin and laboratory aged asphalt binders' study are as follows:

- The evolution of aged asphalt binder physical properties correspond to an evolution in the ESEM microstructure of the binders, as stiffer binders correspond to a denser microstructure.
- Asphalt binders with similar physical properties can have different ESEM 'fingerprints', which will also evolve with aging in different ways.
- The parameters of 'fibril area' and 'formation time' in ESEM generally have a good correlation with the evolution of physical properties in the asphalt binder, although the 'formation time' is not applicable for some binders.
- While the RTFOT aging temperature has some effect on the microstructure evolution, the main microstructural evolution appears after PAV aging.

References

[1] Redelius P, Soenen H. Relation between bitumen chemistry and performance. Fuel 2015;140:34–43. https://doi.org/10.1016/j.fuel.2014.09.044.
[2] Zaumanis M, Mallick RB, Poulikakos L, Frank R. Influence of six rejuvenators on the performance properties of Reclaimed Asphalt Pavement (RAP) binder and 100% recycled asphalt mixtures. Constr Build Mater 2014;71:538–50. https://doi.org/10.1016/j.conbuildmat.2014.08.073.
[3] Petersen JC. A review of the fundamentals of asphalt oxidation: chemical, physicochemical, physical property, and durability relationships. Transp Res E-Circ; 2009.
[4] Rozeveld SJ, Shin EE, Bhurke A, France L, Drzal LT. Network morphology of straight and polymer modified asphalt cements. Microsc Res Tech 1997;38:529–43. https://doi.org/10.1002/(SICI)1097-0029(19970901)38:5<529::AID-JEMT11>3.0.CO;2-O.
[5] Goodhew PJ, Humphreys J, Beanland R. Electron microscopy and analysis. CRC Press; 2000.
[6] Mikhailenko P, Kou C, Baaj H, Tighe S. Observation of Polymer Modified Asphalt Microstructure by ESEM. 6th Int. Conf. Eng. Mech. Mater. CSCE 2017, Vancouver, Canada; 2017.
[7] Stangl K, Jager A, Lackner R. Microstructure-based identification of bitumen performance. Road Mater Pavement Des Int J 2006;7:111–42.
[8] Mikhailenko P, Kadhim H, Baaj H, Tighe S. Observation of asphalt binder microstructure with ESEM. J Microsc 2017;267:347–55. https://doi.org/10.1111/jmi.12574.
[9] On Gaskin J. bitumen microstructure and the effects of crack healing PhD thesis University of Nottingham; 2013.
[10] Mikhailenko P, Kadhim H, Baaj H. Observation of bitumen microstructure oxidation and blending with ESEM. Road Mater Pavement Des 2017;18:216–25. https://doi.org/10.1080/14680629.2017.1304251.
[11] Lu X, Sjövall P, Soenen H, Andersson M. Microstructures of bitumen observed by environmental scanning electron microscopy (ESEM) and chemical analysis using time-of-flight secondary ion mass spectrometry (TOF-SIMS). Fuel 2018;229:198–208. https://doi.org/10.1016/j.fuel.2018.05.036.
[12] Grubb DT. Radiation damage and electron microscopy of organic polymers. J Mater Sci 1974;9:1715–36. https://doi.org/10.1007/BF00540772.
[13] Goldstein J, Newbury DE, Echlin P, Joy DC, Romig Jr AD, Lyman CE, et al. Scanning electron microscopy and X-ray microanalysis: a text for biologists, materials scientists, and geologists. Springer Science & Business Media; 2012.
[14] Mikhailenko P. Valorisation of by-products and products from agro-industry for the development of release and rejuvenating agents for bituminous materials PhD thesis Universite Paul Sabatier Toulouse III; 2015
[15] Egerton RF, Li P, Malac M. Radiation damage in the TEM and SEM. Micron 2004;35:399–409. https://doi.org/10.1016/j.micron.2004.02.003.
[16] Heavens JW, Keller A, Pope JM, Rowell DM. Beam-induced changes in the scanning electron microscopy of poly(oxymethylene). J Mater Sci 1970;5:53–62. https://doi.org/10.1007/PL00020255.
[17] Isaacson M, Johnson D, Crewe AV. Electron beam excitation and damage of biological molecules; its implications for specimen damage in electron microscopy. Radiat Res 1973;55:205–24. https://doi.org/10.2307/3573678.

[18] Hofko B, Falchetto AC, Grenfell J, Huber L, Lu X, Porot L, et al. Effect of short-term ageing temperature on bitumen properties. Road Mater Pavement Des 2017;18:108–17. https://doi.org/10.1080/14680629.2017.1304268.
[19] Migliori F, Corté J-F. Comparative study of RTFOT and PAV aging simulation laboratory tests. Transp Res Rec J Transp Res Board 1998:56–63.
[20] Shaw MT, MacKnight WJ. Introduction to polymer viscoelasticity. John Wiley & Sons; 2005.
[21] Christensen RM. Theory of viscoelasticity. 2nd ed. Courier Corporation; 2013.
[22] Marasteanu MO, Anderson DA. Improved model for bitumen rheological characterization. In: Eurobitume Workshop Perform. Relat. Prop. Bitum. Bind., European Bitumen Association Brussels, Belgium; 1999.
[23] Kou C, Kang A, Zhang W. Methods to prepare polymer modified bitumen samples for morphological observation. Constr Build Mater 2015;81:93–100. https://doi.org/10.1016/j.conbuildmat.2015.01.081.